Pergamon

Int. J. Heat Mass Transfer. Vol. 41, No. 2, pp. 293–302, 1998

Printed in Great Britain
0017–9310/98 $19.00+0.00

PII: S0017-9310(97)00141-5

Mixed convection of air between two horizontal concentric cylinders with a cooled rotating outer cylinder

JOO-SIK YOO

Department of Mechanical Engineering Education, Andong National University, 388 Songchun-dong, Andong, Kyungpuk, 760-749, Korea

(*Received* 4 *February* 1997 *and in final form* 10 *May* 1997)

Abstract—Mixed convection of air with $Pr = 0.7$ between two horizontal concentric cylinders which are held at different uniform temperatures is numerically investigated. The forced flow is induced by the cold outer cylinder which is rotating slowly with constant angular velocity with its axis at the center of annulus. Investigations are made for various combinations of Ra, Re and σ (=diameter of inner cylinder/gap width) in the range of $Ra \leqslant 5 \times 10^4$, $Re \leqslant 1500$, and $0.5 \leqslant \sigma \leqslant 5$. The flow patterns can be categorized into three basic types according to the number of eddies: two-eddy, one-eddy, and no-eddy flows. A map of the three flow regimes is constructed on the Ra–Re plane. Characteristics of flow patterns and heat transfer are elucidated. © 1997 Elsevier Science Ltd.

INTRODUCTION

The fluid flow and the heat transfer in an annulus between two horizontal concentric cylinders have attracted considerable attention because of the theoretical interest and its wide engineering applications such as thermal energy storage systems, cooling of electronic components, and transmission cables. Comprehensive reviews on the study of natural convection phenomena were presented by Kuehn and Goldstein [1], and Gebhart *et al.* [2]. The flow features of natural convection of a fluid with high Prandtl number (of order 1 or larger) have been disclosed experimentally and numerically. Powe *et al.* [3, 4] and Rao *et al.* [5] investigated flow patterns. They found that the free convective flow of a high Prandtl number fluid can be categorized into four basic types: a steady two-dimensional flow with two crescent-shaped eddies, a two-dimensional oscillatory flow, a three-dimensional spiral flow, and a two-dimensional multicellular flow. Recently, Yoo [6] investigated the existence of dual steady states for a fluid of Prandtl number 0.7 (air).

Thermal convection of fluids with low Prandtl number such as liquid metals, exhibits multicellular flow patterns for high Rayleigh numbers [7–11]. In particular, Fant *et al.* [10] and Yoo *et al.* [11] observed oscillatory like-rotating multicellular flow patterns that originated from the hydrodynamic type of instability.

Some other authors have considered a non-uniformly heated annular fluid layer [12], the condition of a constant heat flux at the inner cylinder [13], a conjugate problem [14], cold water [15], and transient convection [16, 17].

In this numerical study, a two-dimensional mixed-convection problem in a horizontal annulus is investigated. The inner cylinder is hotter than the outer one, and the forced flow is induced by the outer cylinder which is rotating slowly with constant angular velocity with its axis at the center of annulus. Up to date, most works for mixed-convection problems in rotating systems have been performed for the flows in vertical cylindrical annuli [18–20]. Relatively few studies, however, have been made for the flows in horizontal annuli. A few authors [21–23] have studied mixed-convective flows within a horizontal annulus with a heated rotating inner cylinder. When the inner cylinder or both of the inner and outer cylinders are rotating, the centrifugal effects created by the rotating cylinder can lead to three-dimensional flows with Taylor vortices [24]. Fusegi *et al.* [21] and Lee [22, 23] purposely limited the calculations to a range of parameters that would exclude this possibility. They considered a few cases of parameters; and the transition phenomena of flow patterns and the effect of aspect ratio were not investigated. On the contrary, the Couette flow between two horizontal concentric cylinders, with the stationary inner cylinder and the outer cylinder rotating about its axis at constant angular velocity (Ω) is proved to be stable, according to linear stability theory, for all values of Ω [24]. When the inner cylinder or both of the inner and outer cylinders are rotating, however, the linear stability theory tells that the flow is not always stable for all values of Ω. It thus appears that a mixed-convection system with the stationary inner cylinder and the outer cylinder rotating is an appropriate configuration to investigate the effect of forced flow on the two-dimensional natural convection in a horizontal annulus. There is, of course, a possibility of three-dimensional flows for

NOMENCLATURE

D_i	diameter of inner cylinder
$\mathbf{e}_r$, $\mathbf{e}_\phi$	unit vectors in the radial and angular directions, respectively
g	acceleration of gravity
J	Jacobian
L	gap width of the annulus, $R_o - R_i$
Nu_{cond}	Nusselt number of pure conduction state
Nu_i, Nu_o	local Nusselt numbers at the inner and outer cylinders, respectively
$\overline{Nu_i}$, $\overline{Nu_o}$	mean Nusselt numbers at the inner and outer cylinders, respectively
$\overline{Nu}$	overall Nusselt number, $(\overline{Nu_i}+\overline{Nu_o})/2$
Pr	Prandtl number, ν/χ
p	dimensionless pressure
Q	net circulation of fluid in the direction of cylinder's rotation, $\lvert\Psi_2-\Psi_1\rvert$
R_i, R_o	radii of the inner and outer cylinders, respectively
Ra	Rayleigh number based on the gap width, $\alpha g(T_i-T_o)L^3/\chi\nu$
Re	Reynolds number, $R_o\Omega L/\nu$
Re_c	critical Reynolds number at which transition of flow pattern occurs
r	dimensionless radial coordinate
r_i, r_o	dimensionless radii of the inner and outer cylinders, respectively
TQ	normalized torque loaded at the outer cylinder with respect to the torque obtained with the Couette velocity distribution
t	dimensionless time
T_i, T_o	temperatures at the inner and outer cylinders, respectively
$\mathbf{u}$	dimensionless velocity vector
u, v	dimensionless velocity components in the radial and angular directions, respectively.

Greek symbols

α	coefficient of thermal expansion
η	stretched coordinate in the radial direction
θ	dimensionless temperature
χ	thermal diffusivity
ν	kinematic viscosity
ρ_0	mean density
σ	ratio of the inner cylinder diameter to gap width, D_i/L
ϕ	angular coordinate
Ψ	dimensionless streamfunction
Ψ_1, Ψ_2	values of the streamfunction at the inner and outer cylinders, respectively
Ω	angular velocity of the outer cylinder
ω	dimensionless vorticity.

nonlinear disturbances at sufficiently high Ra and Re. In the mixed-convection problem, the forced flow can aid or oppose the buoyancy-induced flow. In the present configuration, both aiding and opposing effects exist.

The objective of the present study is to investigate the effect of forced flow induced by the rotating outer cylinder on the characteristics of heat transfer and fluid flow of the two-dimensional natural convection within a horizontal annulus. Investigations are made for various combinations of Ra, Re and σ in the range of $Ra \leqslant 5\times10^4$, $Re \leqslant 1500$ and $0.5 \leqslant \sigma \leqslant 5$ with $Pr = 0.7$. Unlike the case of rotating inner cylinder [21–23], the flow patterns can be categorized into three types according to the number of eddies: two-, one- and no-eddy flows. It would be of interest to investigate the transition phenomena of flow patterns and the characteristics of heat transfer. This study has computed numerous cases of the parameters, and a map of steady-state flow regimes on the Ra–Re plane has been constructed. Characteristics of flow patterns and heat transfer at the walls are elucidated. It is observed that the variation of overall heat transfer with respect to the angular velocity of cylinder is closely related to the flow patterns. For the relatively small Reynolds number in the regime of two-eddy flow, the rotation of cylinder has little effect on the overall heat transfer at the walls, although the distribution of local Nusselt number is significantly altered from that of pure natural convection. As Re approaches the transitional value between two- and one-eddy flows, however, the overall heat transfer is drastically reduced. The transitional Reynolds number between two- and one-eddy flows for small Rayleigh number is not greatly affected by the geometrical parameter of concentric annulus ($0.5 \leqslant \sigma \leqslant 5$).

ANALYSIS

The geometry of the problem and the coordinate system are shown in Fig. 1. The fluid is contained between two infinite horizontal concentric circular cylinders, which are held at different uniform temperatures of T_i and T_o ($T_i > T_o$). The inner cylinder is fixed, but the outer cylinder is rotating slowly in the counter-clockwise direction with constant angular velocity (Ω). Density change in the fluid is neglected everywhere except in the buoyancy, and all the other physical properties of the fluid are assumed constant (Boussinesq approximation). Viscous dissipation in the energy equation is also neglected. We consider a two-dimensional problem, and use the cylindrical

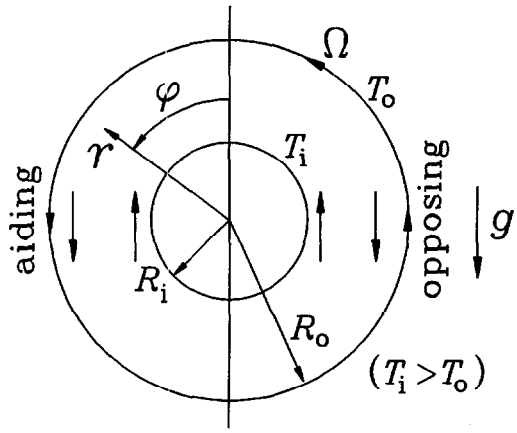

Fig. 1. Problem configuration.

coordinates (r, ϕ), the angular coordinate ϕ being measured counter-clockwise from the upward vertical through the center of the cylinders (Fig. 1). The equations governing conservation of mass, momentum and energy are put into non-dimensional form by taking the characteristic length, time, velocity, pressure, and temperature as L, L/V, $V = R_o\Omega$, $\rho_0 V^2$, and $(T_i - T_o)$, respectively. We let $Pr = \nu/\chi$, $Re = R_o\Omega L/\nu$, and $Ra = \alpha g(T_i - T_o)L^3/\chi\nu$ denote the Prandtl, Reynolds and Rayleigh numbers, respectively. The dimensionless governing equations are

$$\nabla \cdot \mathbf{u} = 0 \tag{1}$$

$$\frac{\partial \mathbf{u}}{\partial t} + (\mathbf{u}\cdot\nabla)\mathbf{u} = -\nabla p + \frac{1}{Re}\nabla^2\mathbf{u} + \frac{Ra}{PrRe^2}\theta[\cos(\phi)\mathbf{e}_r - \sin(\phi)\mathbf{e}_\phi] \tag{2}$$

$$\frac{\partial \theta}{\partial t} + (\mathbf{u}\cdot\nabla)\theta = \frac{1}{PrRe}\nabla^2\theta \tag{3}$$

with the boundary conditions

$$u = v = 0, \quad \theta = 1 \quad \text{at} \quad r = r_i \tag{4}$$

$$u = 0, \quad v = 1, \quad \theta = 0 \quad \text{at} \quad r = r_o. \tag{5}$$

On the introduction of the streamfunction Ψ, continuity equation (1) is satisfied identically. And the dimensionless equations governing the two-dimensional convection in terms of the vorticity ω and streamfunction Ψ are written as follows:

$$\frac{\partial \omega}{\partial t} = J(\Psi, \omega) + \frac{1}{Re}\nabla^2\omega - \frac{Ra}{PrRe^2}\left[\sin(\phi)\frac{\partial\theta}{\partial r} + \cos(\phi)\frac{\partial\theta}{r\,\partial\phi}\right] \tag{6}$$

$$\omega = -\nabla^2\Psi \tag{7}$$

$$\frac{\partial \theta}{\partial t} = J(\Psi, \theta) + \frac{1}{PrRe}\nabla^2\theta \tag{8}$$

where the vorticity ω, streamfunction Ψ, Jacobian $J(f,g)$, and Laplacian ∇^2 are

$$\omega = \frac{\partial}{r\,\partial r}(rv) - \frac{\partial}{r\,\partial\phi}(u), \quad u = \frac{\partial\Psi}{r\,\partial\phi},$$

$$v = -\frac{\partial\Psi}{\partial r}, \quad J(f,g) = \frac{1}{r}\left(\frac{\partial f}{\partial r}\frac{\partial g}{\partial\phi} - \frac{\partial f}{\partial\phi}\frac{\partial g}{\partial r}\right)$$

$$\nabla^2 = \frac{\partial}{r\,\partial r}\left(r\frac{\partial}{\partial r}\right) + \frac{\partial^2}{r^2\,\partial\phi^2}. \tag{9}$$

The boundary conditions on the two walls are

$$\Psi = \Psi_1, \quad \frac{\partial\Psi}{\partial r} = 0, \quad \omega = -\frac{\partial^2\Psi}{\partial r^2}, \quad \theta = 1 \quad \text{at} \quad r = r_i \tag{10}$$

$$\Psi = \Psi_2, \quad \frac{\partial\Psi}{\partial r} = -1, \quad \omega = -\frac{\partial^2\Psi}{\partial r^2} + \frac{1}{r_o}, \quad \theta = 0 \quad \text{at} \quad r = r_o. \tag{11}$$

In the above boundary conditions (10) and (11), values of the streamfunctions, Ψ_1 and Ψ_2 are not given, but are to be determined. In the present problem, we can let $\Psi_1 = 0$ without loss of generality, and Ψ_2 is determined to satisfy the condition of the single value of pressure on the wall [25]. On the surface of the wall where $u = 0$ and $v =$ constant, the following equation is derived from the azimuthal component of momentum equation.

$$\frac{1}{r}\frac{\partial p}{\partial\phi} = \frac{1}{Re}\frac{\partial\omega}{\partial r} - \frac{Ra}{PrRe^2}\theta\sin\phi. \tag{12}$$

Integration along the surface of wall yields

$$I_w \equiv p(r, 2\pi) - p(r, 0) = \int_0^{2\pi}\frac{1}{Re}\left(\frac{\partial\omega}{\partial r}\right)r\,d\phi = 0 \tag{13}$$

because $\theta =$ constant on the wall.

The dimensionless heat transfer rate of pure conduction in the absence of fluid motion is:

$$Nu_{cond} = \frac{1}{\ln(r_o/r_i)}. \tag{14}$$

The local Nusselt number is defined as the actual heat flux divided by $Nu_{cond.}$

$$Nu_i(\phi) = -\left(r\frac{\partial\theta}{\partial r}\right)\Big/ Nu_{cond} \quad \text{at } r = r_i \tag{15}$$

$$Nu_o(\phi) = -\left(r\frac{\partial\theta}{\partial r}\right)\Big/ Nu_{cond} \quad \text{at } r = r_o \tag{16}$$

and the mean Nusselt numbers, $\overline{Nu_i}$ and $\overline{Nu_o}$, are given by

$$\overline{Nu_i} = \frac{1}{2\pi}\int_0^{2\pi} Nu_i(\phi)\,d\phi \tag{17}$$

$$\overline{Nu_o} = \frac{1}{2\pi}\int_0^{2\pi} Nu_o(\phi)\,d\phi. \quad (18)$$

In steady states, $\overline{Nu_i}$ and $\overline{Nu_o}$ are presumably of the same value.

Equations (6)–(13) are numerically solved by the similar finite difference scheme used in Yoo and Kim [26] for spatially periodic flow. Equations (6) and (8) are cast into finite difference form using the leap-frog method [27] of Dufort–Frankel for the diffusion and time derivative terms, and central differencing for the Jacobian. The Poisson equation for the steamfunction is discretized by use of five-point formula. Because the computational domain is rectangular, the discretized Poisson equation is solved by the direct method of Buzbee *et al.* [28] which uses cyclic even–odd reduction method. The algorithm of Buzbee *et al.* [28] is known to be extremely fast and accurate. In the azimuthal direction, a uniform grid is employed, and in the radial direction, the following coordinate stretching is utilized.

$$r = r_i + \frac{1}{2}\left[1 + \frac{\tanh\{C(2\eta-1)\}}{\tanh(C)}\right]$$

$$\text{with } C = 1.5, \quad 0 \leqslant \eta \leqslant 1. \quad (19)$$

The solution was considered to have converged to the steady state, when the absolute value of the maximum relative difference between two consecutive time steps was less than a prescribed value ε:

$$\text{Max}\left|\frac{f_{i,j}^{n+1} - f_{i,j}^{n}}{f_{i,j}^{n+1}}\right| < \varepsilon \quad \text{for } f = \omega, \quad \Psi$$

$$\text{and} \quad \theta \quad \text{with } \varepsilon < 10^{-3}.$$

For most cases, ε was set equal to 10^{-4}. The time step Δt was taken in the range of $10^{-5} < \Delta t < 5\times10^{-3}$. At the initial stage, a small time step $\Delta t \simeq 10^{-5}$ was used, and later on Δt was changed to a larger value $\Delta t \simeq 10^{-3}$. According to the values of inverse relative gap width (σ) and Rayleigh number (Ra), different grids were used: the $(r\times\phi)$ meshes of (65×64), (45×64), or (65×32).

RESULTS AND DISCUSSION

Computations were performed for various combinations of Ra, Re and σ in the range of $Ra \leqslant 5\times10^4$, $Re \leqslant 1500$, and $0.5 \leqslant \sigma \leqslant 5$, with $Pr = 0.7$. The main investigations were made for an annulus of $\sigma = 2$. To check the numerical method, the problem of pure forced convection ($Ra = 0$) and that of pure natural convection were solved. The two-dimensional forced convection problem yields the circular Couette flow with $u = 0$, $v = V(r)$, and $p = P(r)$, where $V(r)$ is determined from the azimuthal component of momentum equation. The solution is

$$V(r) = Ar + \frac{B}{r} \quad (20)$$

where

$$A = \frac{r_o}{r_o^2 - r_i^2}, \quad B = -\frac{r_o r_i^2}{r_o^2 - r_i^2}.$$

This gives

$$-\Psi_2 = \int_{r_i}^{r_o} V(r)\,dr = A(r_o^2 - r_i^2)/2 + B\ln(r_o/r_i). \quad (21)$$

Some values of the numerically calculated Ψ_2 for $\sigma = 2$ are listed in Table 1. It shows that as the number of grid points is increased, the error approaches zero. We can see that the $(r\times\phi)$ grid of (35×32) yields sufficiently accurate result. This study, however, used 65-grid points in the radial direction, for most cases, to resolve the thin boundary layer near the outer cylinder sufficiently. The results of the pure natural convection problem were compared with those obtained by Kuehn and Goldstein [1]. They showed good agreement with each other.

Firstly, the flow patterns for small Rayleigh number are presented. The flow field induced by pure buoyancy force consists of two kidney-shaped eddies which are symmetric with respect to the vertical axis $\phi = 0$. When the outer cylinder is rotating, the symmetry is broken. The variation of flow patterns with respect to Reynolds number is shown in Fig. 2 for $\sigma = 2$ and $Ra = 1000$. For small Reynolds number, the two symmetric eddies created by the pure buoyancy force are slightly altered by the forced convection [Fig. 2(a)]. There is net circulation of fluid around both of the inner and outer cylinders. The circulation for small Rayleigh number ($Ra < 1000$) is smooth and is similar to that observed by Wang and Bau [29] in the natural convection of low Rayleigh number in an eccentric annulus. In the region of $\pi < \phi < 2\pi$, the forced flow near the outer cylinder opposes the buoyancy-induced flow. The eddy in that region, however, persists when the forced flow is weak. As Reynolds number increases, the eddy becomes more strongly suppressed by the forced flow [Fig. 2(b)], and above a certain critical value it disappears [Fig. 2(c)]. At the higher

Table 1. Numerically determined values of Ψ_2 when $Ra = 0$ and $\sigma = 2$ with 32-grid points to the azimuthal direction

Number of r-grid points	Calculated $-\Psi_2$	Percent error
15	0.5474	1.766
25	0.5413	0.632
35	0.5396	0.316
45	0.5389	0.186
55	0.5386	0.130
Exact	0.5379	—

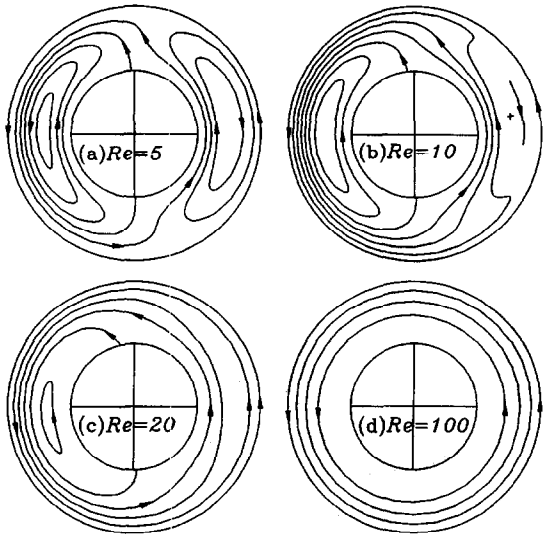

Fig. 2. Streamlines for several Reynolds numbers when $\sigma = 2$ and $Ra = 1000$: (a) $Re = 5$; (b) $Re = 10$; (c) $Re = 20$; (d) $Re = 100$. The cross in (b) indicates the center of weak eddy.

Reynolds number, the remaining eddy in $0 < \phi < \pi$ also disappears [Fig. 2(d)].

As Ra is increased, the circulation of fluid around the inner cylinder becomes complex. The flow patterns at $Ra = 10^4$ with $\sigma = 2$ are presented in Fig. 3. For $Ra \leqslant 10^4$, the streamline of $\Psi = 0$, which separates the two eddies always encompasses the large eddy, and with increased speed of rotation the separation point on the upper portion of inner cylinder moves in the direction of cylinder's rotation. When $Ra \geqslant 2 \times 10^4$, however, the separating streamline does not always encompass the large eddy, and the separation point does not always move in the same direction of cylinder's rotation with increased speed of rotation. For example, the flow patterns at $Ra = 5 \times 10^4$ are presented in Fig. 4. When $Re = 100$, the point of Ψ_{max} (indicated by the cross) locates in the upper portion of annulus [Fig. 4(a)]. As Re is increased, it moves in the direction of cylinder's rotation, and the large eddy grows further in size. During this course, the separating streamline on the top of annulus becomes to be deflected right due to the increased drag of large eddy in the right side of annulus [Fig. 4(b)]. And finally, the separating streamline of $\Psi = 0$ encompasses the small eddy, at $Re = 400$ [Fig. 4(c)]. For $Re \leqslant 600$ [Fig. 4(d)], with increase of Re the separation point on the inner cylinder moves in the opposite direction of cylinder's rotation. This is caused by the increased drag of large eddy. As Re is increased further, however, the separation point moves in the same direction of cylinder's rotation [Fig. 4(e)]. Finally, the small eddy disappears, and the streamline of $\Psi = 0$ encompasses the remaining eddy, at $Re = 900$ [Fig. 4(f)].

The isotherms presented in Figs 3 and 4 also show the above characteristics well. It is interesting that

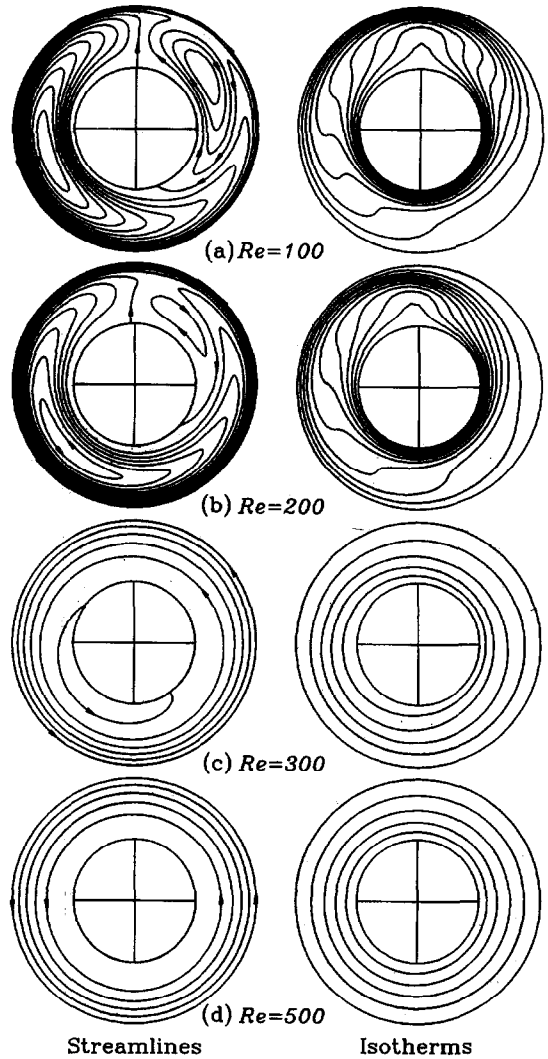

Fig. 3. Streamlines and isotherms for several Reynolds numbers when $\sigma = 2$ and $Ra = 10^4$: (a) $Re = 100$; (b) $Re = 200$; (c) $Re = 300$; (d) $Re = 500$.

the thermal plumes near the upper portion of inner cylinder for $Ra = 5 \times 10^4$ in Fig. 4(b–d) are tilted in the opposite direction of cylinder's rotation. For small Rayleigh number ($Ra \leqslant 10^4$), the thermal plume is always tilted in the same direction of cylinder's rotation (Fig. 3). In general, the forced flow tends to stratify the temperature field in the radial direction. It is to be noted that the isotherms of one-eddy flow constitute nearly concentric circles.

As shown in Figs 2–4, the flows can be categorized into three different patterns according to the number of eddies: two eddies [Fig. 2(a)], one eddy [Fig. 2(c)], and no eddy [Fig. 2(d)]. The map of the three flow regimes for $\sigma = 2$ is presented in Fig. 5. In the conduction-dominated regime of $Ra < 1000$, the boundary lines are approximated as $Re = C_1 Ra^{C_2}$. The approximate values of C_1 and C_2 are $(C_1, C_2) = (0.009, 1.08)$ and $(0.13, 0.95)$ for the transition between two- and one-eddy flows and that between one- and no-

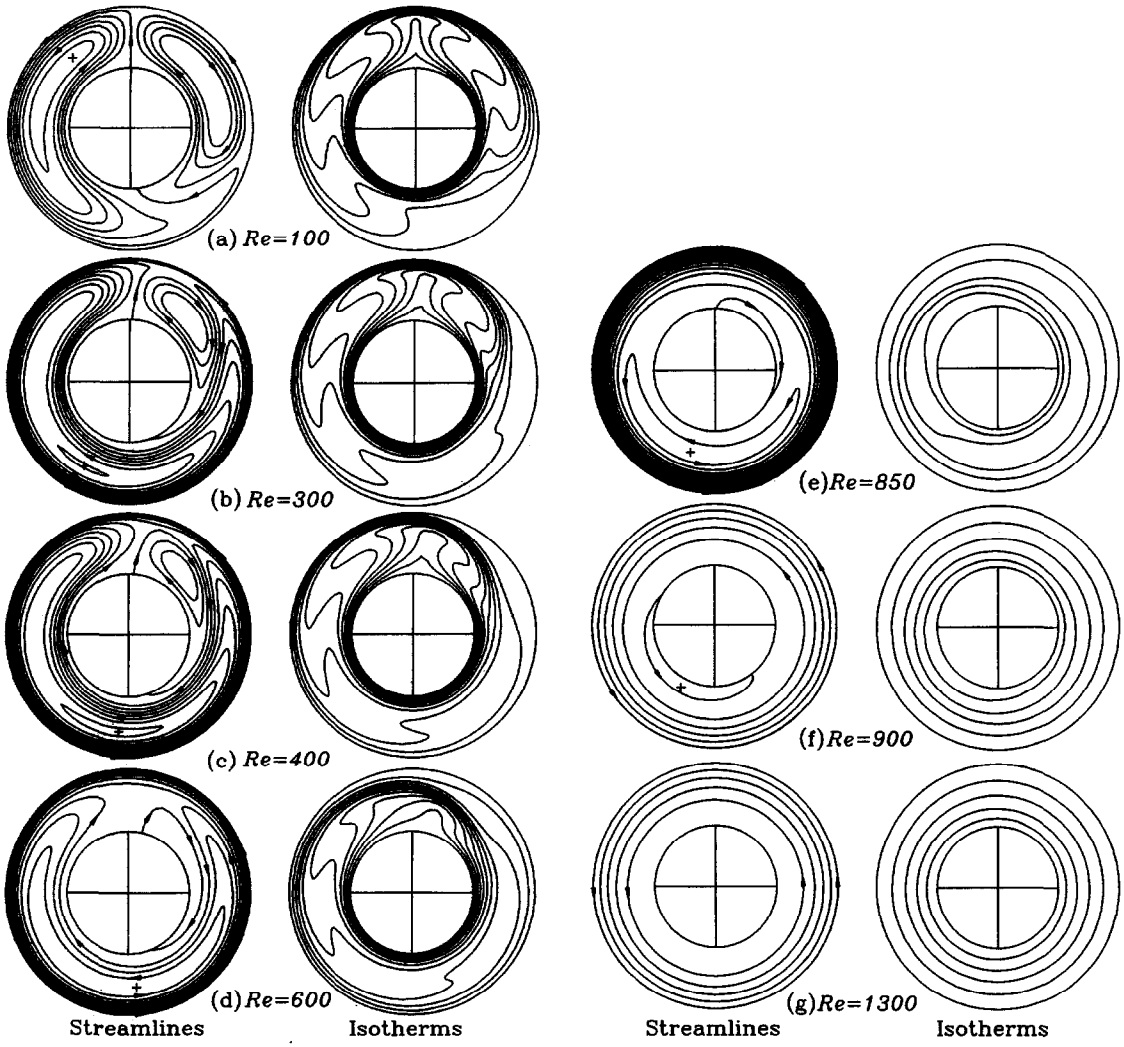

Fig. 4. Streamlines and isotherms for several Reynolds numbers when $\sigma = 2$ and $Ra = 5 \times 10^4$: (a) $Re = 100$; (b) $Re = 300$; (c) $Re = 400$; (d) $Re = 600$; (e) $Re = 850$; (f) $Re = 900$; (g) $Re = 1300$. The cross in the plot of streamlines indicates the point of Ψ_{max}.

eddy flows, respectively. As Ra is increased, the transitional Reynolds number between two- and one-eddy approaches that between one- and no-eddy.

The flow patterns have been investigated carefully with the plots of streamlines and angular velocity of fluid. For a fixed Rayleigh number, a solution for a small Reynolds number was obtained, and for most cases, the solution at the higher Reynolds number was found by letting the initial conditions be the solution of lower Re previously obtained. It has also been tried to obtain the solutions for lower Re flows from the previously obtained higher Re flow solutions. Both methods yielded identical results for the same parameters. That is, hysteresis phenomena have not been observed.

In the mixed-convective system, the forced flow can aid or oppose the buoyancy-induced flow. In the present configuration, both aiding and opposing effects exist (Fig. 1). The distributions of angular velocities at $\phi = \pi/2$ and $3\pi/2$ are presented in Fig. 6 for $Ra = 100$, 1000, 2000, 5000 and 10 000, with $Re = 20$ and $\sigma = 2$. There appears no-eddy at $Ra = 100$, but one-eddy at $Ra = 1000$, and two-eddies at $Ra = 2000$, 5000 and 10 000: for a fixed Reynolds number, there occur transitions of flow patterns from no- to one-eddy and from one- to two-eddies, as Ra increases (Fig. 5). All the fluid move in the direction of cylinder's rotation for small Rayleigh number. At $Ra = 100$, the velocity distribution is nearly identical to that of Couette flow. As Ra increases, the velocity profile becomes increasingly skewed by buoyancy force, and the slope of the velocity distribution near the walls becomes steep. At a large Rayleigh number, the velocity at $\phi = \pi/2$ adjacent to the hot inner cylinder becomes negative [Fig. 6(a)—$Ra = 1000$], and the velocity at $\phi = 3\pi/2$ also becomes negative at the higher Rayleigh number [Fig. 6(b)—$Ra = 2000$, 5000, 10 000]. The variation of the velocity profile with respect to Rayleigh number (Fig. 6)

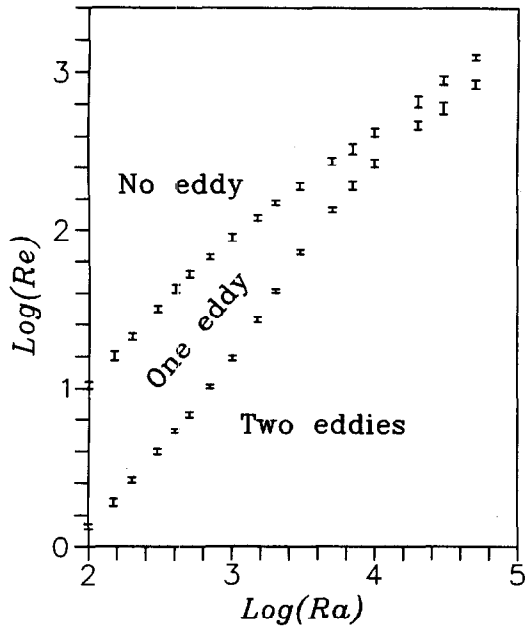

Fig. 5. Classification of flow regimes according to the number of eddies on the *Ra*–*Re* plane when $\sigma = 2$. The transition of flow patterns occurs at the Reynolds number betwen the error brackets.

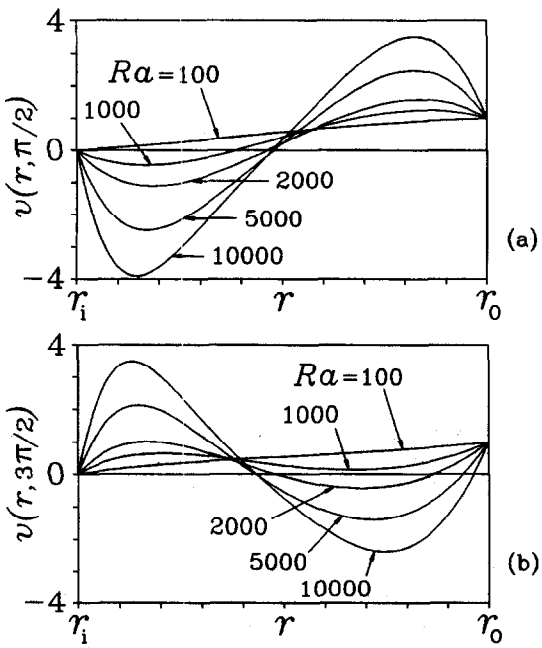

Fig. 6. Distribution of angular velocities at $\phi = \pi/2$ (a) and $\phi = 3\pi/2$ (b) as a function of Rayleigh number when $\sigma = 2$ and $Re = 20$.

resembles that observed by Aung and Worku [30, 31] in the mixed convection in a vertical channel, in which flow reversal similar to that in Fig. 6(a) was found.

Up to this point, the case of $\sigma = 2$ has been presented. And similar characteristics of flow patterns in the number of eddies have been observed for the other geometric configurations of annuli. The cases

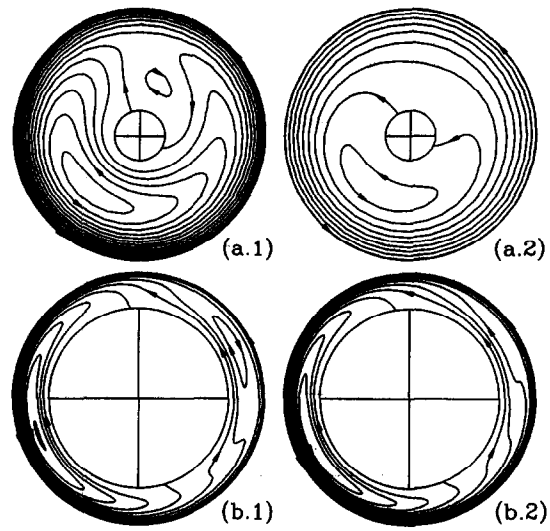

Fig. 7. Two-eddy and one-eddy flow patterns at $Ra = 5000$ for wide and narrow annuli: (a.1) $\sigma = 0.5$, $Re = 100$; (a.2) $\sigma = 0.5$, $Re = 120$; (b.1) $\sigma = 5$, $Re = 100$; (b.2) $\sigma = 5$, $Re = 130$.

of $\sigma = 0.5$ (wide gap) and $\sigma = 5$ (narrow gap) are presented in Fig. 7, which represents two- and one-eddy flow patterns. For $\sigma = 0.5$, the convective fluid has more space to move around and the fluid motion and heat transfer characteristics tend to be more convective like. For $\sigma = 5$, the fluid enclosed by the separating streamline of $\Psi = 0$ has less space to move about and the fluid motion and heat transfer behavior tend to be more conduction like.

The dependencies of the critical Reynolds numbers at which transitions of flow patterns occur on the geometric parameters (σ) are presented in Fig. 8 for $Ra = 200$, 1000 and 5000. Figure 8(a) represents the curves of the critical Reynolds number (Re_c) between two- and one-eddy flows, and Fig. 8(b) represents those between one- and no-eddy flows. As σ is increased, Re_c between two- and one-eddy flows for $Ra = 200$ is slightly increased, but those have maximum value around $1 < \sigma < 2$ for $Ra = 1000$ and 5000 [Fig. 8(a)]. However, Re_c between one- and no-eddy flows is increased for all Rayleigh numbers [Fig. 8(b)]. Overall, the transitional Reynolds numbers between two- and one-eddy flows for small Rayleigh number are not greatly affected by the geometrical parameter of the concentric annulus.

The net circulation of fluid in the direction of cylinder's rotation ($Q = |\Psi_2 - \Psi_1|$), and the torque (TQ) acting on the outer cylinder are shown in Fig 9. The dimensionless torque is given by

$$\text{Torque} = \int_0^{2\pi} (\tau \cdot r^2)\, d\phi, \quad \tau = r\frac{\partial}{\partial r}\left(\frac{v}{r}\right) \tag{22}$$

and TQ is defined as the actual torque on the outer cylinder divided by the torque obtained with the Couette velocity distribution [equation (20)]. When the Rayleigh number is small, the net circulation and

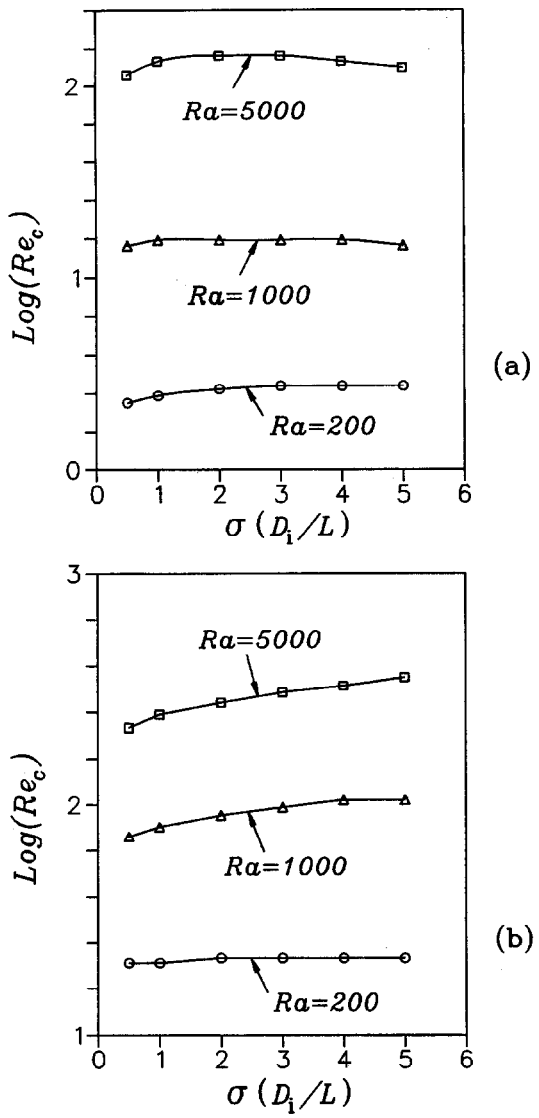

Fig. 8. Critical Reynolds numbers (Re_c) at which transitions of flow patterns occur as functions of σ for several Rayleigh numbers: (a) between two eddy and one eddy; (b) between one eddy and no eddy.

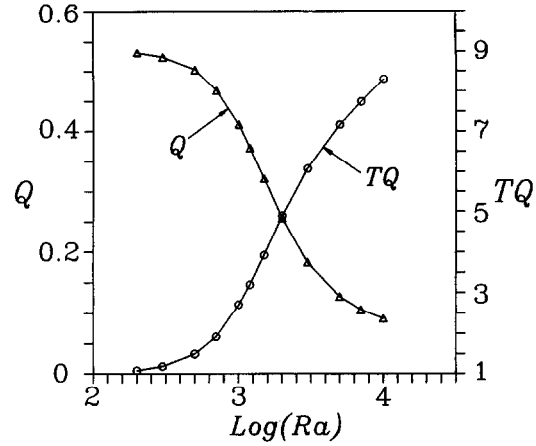

Fig. 9. Net circulation of fluid in the direction of cylinder's rotation ($Q = |\Psi_2 - \Psi_1|$) and the torque (TQ) acting on the outer cylinder as functions of Rayleigh number when $\sigma = 2$ and $Re = 20$.

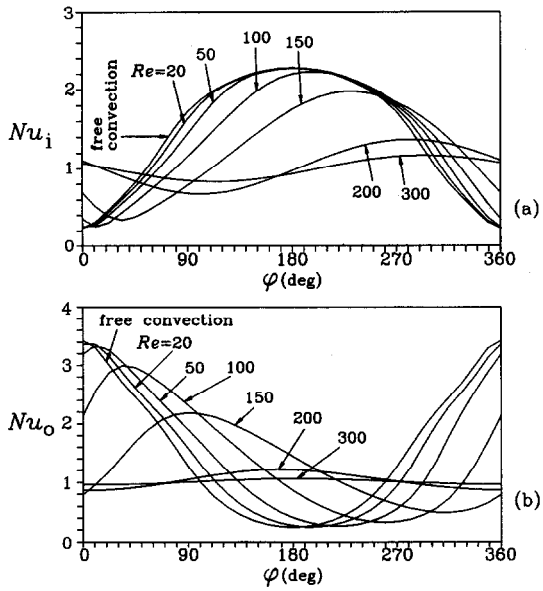

Fig. 10. Variation of local Nusselt number distributions at the inner (a) and outer (b) cylinders with respect to Reynolds number when $\sigma = 2$ and $Ra = 5000$.

the torque are close to those of the Couette flow, $Q = 0.5379$, $TQ = 1$. As Rayleigh number becomes large, the net circulation decreases and approaches zero, but the torque increases due to the strong resisting buoyancy force near the outer cylinder. That is, the free-convective motion of fluid tends to block the circulation of fluid. This behavior can be also seen from the velocity distributions in Fig. 6.

To see the effects of cylinder's rotation on the local heat fluxes, the distributions of local Nusselt numbers at the inner (Nu_i) and other (Nu_o) cylinders for $Ra = 5000$ and $Ra = 5 \times 10^4$ are shown in Figs 10 and 11, with $\sigma = 2$. As the speed of rotation is increased, the points of maximum and minimum local heat fluxes at both of the inner and outer cylinders move in the direction of cylinder's rotation for $Ra = 5000$ (Fig. 10). When $Ra = 5 \times 10^4$ (Fig. 11), however, the points at the inner cylinder do not always move in the same direction: the curves of $Re = 300$, 400, 600 for maximum Nu_i and those of $Re = 100$, 200, 300, 400, 600 for minimum Nu_i show that the points move in the opposite direction of cylinder's rotation. These phenomena correspond to the variation of flow patterns in Fig. 4. Apparently, the distributions of local Nusselt numbers for all Reynolds numbers are different from those of free convection. The cases of $Re = 20$, 50 in Fig. 10 and $Re = 100$ in Fig. 11, however, show that the integrated values of Nu_i (or Nu_o) are nearly identical to the free-convection values.

Finally, the overall Nusselt numbers are shown in Fig. 12 as functions of Reynolds number for

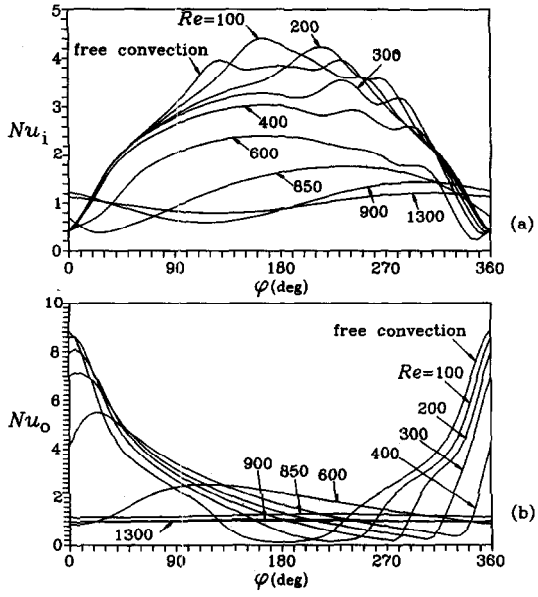

Fig. 11. Variation of local Nusselt number distributions at the inner (a) and outer (b) cylinders with respect to Reynolds number when $\sigma = 2$ and $Ra = 5 \times 10^4$.

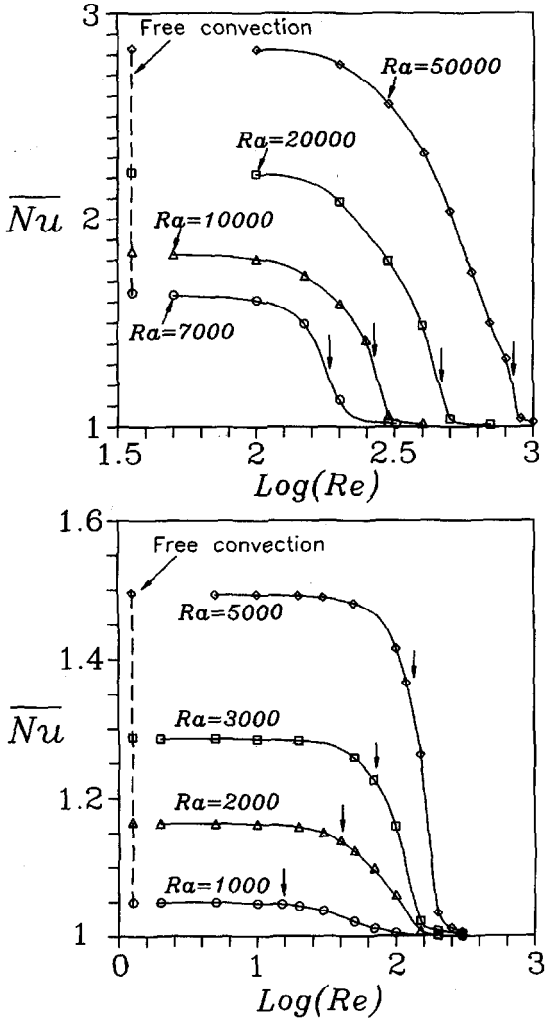

Fig. 12. Overall Nusselt numbers as functions of Reynolds number for several Rayleigh numbers when $\sigma = 2$: $Ra = 1000$, 2000, 3000, 5000, 7000, 10^4, 2×10^4 and 5×10^4. The values on the vertical dashed line represent the Nusselt numbers of pure free convection. The arrows on the curves of Nusselt number indicate the transition Reynolds numbers between two-eddy and one-eddy flow patterns.

$Ra = 1000$, 2000, 3000, 5000, 7000, 10^4, 2×10^4 and 5×10^4 with $\sigma = 2$. The forced flow tends to stratify the temperature field in the radial direction. There is a kind of competition between the buoyancy-induced flow and the forced flow. For small Reynolds number, the Nusselt number is nearly identical to that of free convection, but above a certain Reynolds number it decreases rapidly and approaches unity. The range of the Reynolds number where there is no great variation in heat transfer becomes wide, as Rayleigh number increases. Comparing the map of flow regime (Fig. 5) with the curves of overall Nusselt numbers (Fig. 12), it can be seen that the region of Re in which there is little variation in heat transfer corresponds to the flow regime of strong two eddies. As Re approaches the transitional Reynolds number between two-eddy and one-eddy patterns, however, the overall heat transfer is rapidly decreased. Figures 3 and 4 show that the isotherms of one-eddy flow constitute nearly concentric circles. This implies that the overall Nusselt number at the walls for one-eddy flow is near the value of conduction state.

CONCLUSIONS

Mixed convection in a horizontal concentric annulus was numerically investigated for air with $Pr = 0.7$. The inner cylinder is hotter than the outer cylinder. The forced flow is induced by the cold outer cylinder which is rotating slowly with constant angular velocity with its axis at the center of the annulus. Investigations were made for various combinations of Ra, Re, and σ in the range of $Ra \leqslant 5 \times 10^4$, $Re \leqslant 1500$, and $0.5 \leqslant \sigma \leqslant 5$. The flow patterns can be categorized into three types according to the number of eddies: two-, one- and no-eddy flows. A map of the three flow regimes was constructed on the Ra–Re plane. The transitional Reynolds number between two- and one-eddy flows for small Rayleigh number is not greatly affected by the geometrical parameter of the concentric annulus ($0.5 \leqslant \sigma \leqslant 5$). Net circulation of fluid in the direction of cylinder's rotation is decreased as the Rayleigh number is increased. As the speed of the cylinder's rotation is increased, the points of maximum and minimum local heat fluxes at both of the inner and outer cylinders move in the same direction of cylinder's rotation for small Rayleigh number, but for high Rayleigh number the points at the inner cylinder do not always move in the same direction. Overall heat transfer at the wall is rapidly decreased, as Re approaches the transitional Reynolds number between two- and one-eddy flows.

REFERENCES

1. Kuehn, T. H. and Goldstein, R. J. An experimental and theoretical study of natural convection in the annulus between horizontal concentric cylinders. *Journal of Fluid Mechanics*, 1976, **74,** 695–719.
2. Gebhart, B., Jaluria, Y., Mahajan, R. L. and Sammakia, B., *Buoyancy-induced Flows and Transport*. Hemisphere Publishing Corporation, 1988, pp. 764–771.
3. Powe, R. E., Carley, C. T. and Bishop, E. H., Free convective flow patterns in cylindrical annuli. *Journal of Heat Transfer*, 1969, **91,** 310–314.
4. Powe, R. E., Carley, C. T. and Carruth, S. L., A numerical solution for natural convection in cylindrical annuli. *Journal of Heat Transfer*, 1971, **93,** 210–220.
5. Rao, Y. F., Miki, Y., Fukuda, K., Takata, Y. and Hasegawa, S., Flow patterns of natural convection in horizontal cylindrical annuli. *International Journal of Heat and Mass Transfer*, 1985, **28,** 705–714.
6. Yoo, J.-S., Dual steady solutions in natural convection between horizontal concentric cylinders. *International Journal of Heat and Fluid Flow*, 1996, **17,** 587–593.
7. Mack, L. R. and Bishop, E. H., Natural convection between horizontal concentric cylinders for low Rayleigh numbers. *Quarterly Journal of Mechanics and Applied Mathematics*, 1968, **21,** 223–241.
8. Custer, J. R. and Sharghnessy, E. J., Thermoconvective motion of low Prandtl number fluids within a horizontal cylindrical annulus. *Journal of Heat Transfer*, 1977, **99,** 596–602.
9. Charrier-Mojtabi, M. C., Mojtabi, A. and Caltagirone, J. P., Numerical solution of a flow due to natural convection in horizontal cylindrical annulus. *Journal of Heat Transfer*, 1979, **101,** 171–173.
10. Fant, D. B., Prusa, J. and Rothamayer, A. P., Unsteady multicellular natural convection in a narrow horizontal cylindrical annulus. *Journal of Heat Transfer*, 1990, **112,** 379–387.
11. Yoo, J.-S., Choi, J.-Y. and Kim, M.-U., Multicellular natural convection of a low Prandtl number fluid between horizontal concentric cylinders. *Numerical Heat Transfer, Part A*, 1994, **25,** 103–115.
12. Prud'homme, M, Robillard, L. and Vasseur, P., A study of laminar natural convection in a nonuniformly heated annular fluid layer. *International Journal of Heat and Mass Transfer*, 1987, **30,** 1209–1222.
13. Kumar, P., Study of natural convection in horizontal annuli. *International Journal of Heat and Mass Transfer*, 1988, **31,** 1137–1148.
14. Kolesnikov, P. M. and Bubnovich, V. I., Non-stationary conjugate free-convective heat transfer in horizontal cylindrical coaxial channels. *International Journal of Heat and Mass Transfer*, 1988, **31,** 1149–1156.
15. Ho, C. J. and Lin, Y. H., Laminar natural convection of cold water enclosed in a horizontal annulus with mixed boundary conditions. *International Journal of Heat and Mass Transfer*, 1988, **31,** 2113–2121.
16. Tsui, Y. T. and Tremblay, B., On transient natural convection heat transfer in the annulus between concentric horizontal cylinders with isothermal surfaces. *International Journal of Heat and Mass Transfer*, 1984, **27,** 103–111.
17. Castrejon, A. and Spalding, D. B., An experimental and theoretical study of transient free-convection flow between horizontal concentric cylinders. *International Journal of Heat and Mass Transfer*, 1988, **31,** 273–284.
18. Guo, Z.-Y. and Zhang, C.-M., Thermal drive in centrifugal fields—mixed convection in a vertical rotating cylinder. *International Journal of Heat and Mass Transfer*, 1992, **35,** 1635–1644.
19. Shaarawi, M. A. I. Ei. and Khamis, M., Induced flow in uniformly heated vertical annuli with rotating inner walls. *Numerical Heat Transfer*, 1987, **12,** 493–508.
20. Hessami, M. A., Davis, G. D. V., Lenonardi, E. and Reizes, J. A., Mixed convection in vertical cylindrical annuli. *International Journal of Heat and Mass Transfer*, 1987, **30,** 151–164.
21. Fusegi, T., Farouk, B. and Ball, K. S., Mixed-convection flows within a horizontal concentric annulus with a heated rotating inner cylinder. *Numerical Heat Transfer*, 1986, **9,** 591–604.
22. Lee, T. S., Laminar fluid convection between concentric and eccentric heated horizontal rotating cylinders for low-Prandtl-number fluids. *International Journal for Numerical Methods in Fluids*, 1992, **14,** 1037–1062.
23. Lee, T. S., Numerical computation of fluid convection with air enclosed between the annuli of eccentric heated horizontal rotating cylinders. *Computers and Fluids*, 1992, **21,** 355–368.
24. DiPrima, R. C. and Swinney, H. L., Instabilities and transition in flow between concentric rotating cylinders. In *Topics in Applied Physics*, Vol. 45, ed. H. L. Swinney and J. P. Gollub. Springer, Berlin, 1981, pp. 139–180.
25. Adlam, J. H., Computation of two-dimensional time-dependent natural convection in a cavity where there are internal bodies. *Computers and Fluids*, 1986, **14,** 141–157.
26. Yoo, J.-S. and Kim, M.-U., Two-dimensional convection in a horizontal fluid layer with spatially periodic boundary temperatures. *Fluid Dynamic Research*, 1991, **7,** 181–200.
27. Roache, P. J., *Computational Fluid Dynamics*. Hermosa, 1972, pp. 53–64.
28. Buzbee, B. L., Golub, G. H. and Nielson, C. W., On direct methods for solving Poisson's equations. *SIAM Journal of Numerical Analysis*, 1970, **7,** 627–656.
29. Wang, Y. Z. and Bau, H. H., Low Rayleigh number convection in horizontal, eccentric annuli. *Physics of Fluids*, 1988, **31,** 2467–2473.
30. Aung, W. and Worku, G., Developing flow and flow reversal in a vertical channel with asymmetric wall temperature. *Journal of Heat Transfer*, 1986, **108,** 299–304.
31. Aung, W. and Worku, G., Theory of fully developed, combined convection including flow reversal. *Journal of Heat Transfer*, 1986, **108,** 485–488.